Initial surface roughness influence on the generation of LIPSS on titanium and stainless steel and their effect on cell/bacteria viability

Lamborghini Sotelo[a,b], Tommaso Fontanot[c], Sanjana Vig[d,e], Maria Helena Fernandes[d,e], George Sarau[a,c,f], Gerd Leuchs[f], and Silke Christiansen[a,c,g]

[a]Institute for Nanotechnology and Correlative Microscopy eV INAM, Äußere Nürnberger Str. 62, 91301 Forchheim, Germany
[b]Friedrich-Alexander University Erlangen-Nürnberg, Staudstraße 7, 91058 Erlangen, Germany
[c]Fraunhofer Institute for Ceramic Technologies and Systems IKTS, Äußere Nürnberger Str. 62, 91301 Forchheim, Germany
[d]Faculdade de Medicina Dentaria, Universidade do Porto, Rua Dr. Manuel Pereira da Silva, 4200-393 Porto, Portugal
[e]LAQV/REQUIMTE, University of Porto, 4160-007 Porto, Portugal
[f]Max Planck Institute for Science of Light, Staudstr. 2, 91058 Erlangen, Germany
[g]Frei Universität Berlin, Arnimalle 14, 1495 Berlin, Germany

ABSTRACT

In this work, the influence of initial surface roughness on laser-induced periodic surface structures (LIPSS) formation is explored for titanium and stainless steel samples polished with grain sizes of 18.3μm, 8.4μm, 5μm, and 0.5μm, and lasered maintaining the same irradiation conditions. The resulting structures were studied by scanning electron microscopy (SEM), atomic force microscopy (AFM), Raman spectroscopy, and contact angle (CA) measurements, in order to characterize LIPSS periodicity and orientation, as well as surface chemistry and wettability. After characterization, representative structures were chosen to further explore their potential for bone implant treatment by inducing cells (MG63) and bacteria (*E.coli* and *S.aureus*) and testing for viability by resazurin assays, alkaline phosphatase activity, and SEM imaging. Results show that initial surface roughness (Ra) plays a different role on LIPSS generation for both materials, with stainless steel showing a higher dependence on Ra than titanium, however, both materials show a reduction on bacterial viability, while cell proliferation between polished and lasered samples also show an enhanced osteogenic effect.

Keywords: Laser-Induced Periodic Surface Structures, Stainless Steel, Titanium, Laser functionalization, Biocompatibility

1. INTRODUCTION

An implant material must be accordingly selected to match the implant function and the tissue it will be in contact with. For high stress bearing implants, metals tend to be the common option as they offer a higher load resistance, which makes them suitable for prosthetics facing constant friction and tension, like full limp replacement, hip joints, knee joints, and shoulder replacements.[1,2]

Within the metal options, stainless steel and titanium (along with their alloys) have been widely explored, with some of the first reports dating back to 1940, where titanium and stainless steel plates were implanted on rats with no negative effects.[3]

As stainless steel tends to be cheaper, it took time for titanium to catch up in popularity, gaining traction in the 70s,[4] when some advantages over stainless steel where found. Particularly within the bone implant regime, titanium showed higher implant success ratios as the lower elastic modulus (40-110 GPa) allowed for a better bone

Further author information: (Send correspondence to Lamborghini S.)
Lamborghini S.: E-mail: lamborghini.sotelo@inam-forchheim.de

Laser-based Micro- and Nanoprocessing XVII, edited by Rainer Kling, Akira Watanabe, Wilhelm Pfleging,
Proc. of SPIE Vol. 12409, 124090S · © 2023 SPIE · 0277-786X
doi: 10.1117/12.2648921

coupling, preventing stress shielding and bone resorption, which are more common for stainless steel implants (elastic modulus of 210 GPa).[5]

Titanium and its alloys also show great corrosion resistance due to a passive oxide layer formed on their surface, this TiO_2 film is highly stable and reduces corrosion rates.[6] Stainless steel also forms a protective oxide layer, however this tends to be thinner and leads to surface cracking and break down, which allows for metal oxidation and finally results in implant failure.[7] In order to prevent this, it is possible to deposit a TiO_2 layer on top of titanium and stainless steel to increase the thickness of the naturally formed oxide layer and improve its corrosion resistance.[8]

It has also been shown that surface structuring plays an important role for bacterial and cell adhesion.[9,10] In this sense, laser-induced periodic surface structures (LIPSS) have shown to be a great option for implant surface treatment as they allow for the simultaneous generation of micro and nano patterns to be imprinted on the surface[11–13] that directly affect surface wettability, cell and bacterial adhesion, as well as inducing laser oxidation of metals.[14,15]

Orthopedic implant associated infections represent one of the major post-surgery complications contributing to implant failure. *Staphylococcus aureus*, a gram positive bacterium is one of the most prevalent pathogenic species in orthopedic infections, accounting for more than 30% of total cases.[16] This bacteria possesses several adhesion proteins on the surface that facilitate binding with bone matrix including collagen-binding adhesins, fibronectin-binding adhesins, elastin-binding adhesins and fibrinogen-binding adhesins among others.[17] Infections caused by gram negative bacteria are also clinically relevant even though they are less common. Bone implant infections are initiated by the formation of a biofilm on the implant surface occurring in a multistage process. Initially, the bacteria attach to the surface of implant and secrete matrix extracellular polymeric substances which promote bacterial aggregation in multiple layers. Towards biofilm maturation, some of these bacteria detach to initiate a new cycle of biofilm formation,[18] to then repeat the process described in the previous sentence. The biofilm acts as protective layer to promote persistent, chronic infections while making the bacteria resistant to antibiotics. Production of biomaterials with inherent antibacterial properties is thus crucial for countering post-surgery infections. Laser patterning of biomaterial surfaces to generate antibacterial, nanotopographical structures or LIPSS, is an innovative strategy to prevent biofilm formation on biomaterial surfaces.

2. MATERIALS AND METHODS

2.1 Sample preparation

Stainless steel (1.4301) and titanium plates (HMW hauner GmbH & Co.Kg, Germany) of 10 mm x 10 mm x 0.5 mm size were polished with a grinding machine (EcoMet250, Buehler, Switzerland) using a sequence of SiC paper going from P1000 (grain size 18.3μm), P2500 (grain size 8.4μm), P4000 (grain size 5μm), and finishing with manual polishing using a diamond paste (grain size 0.5μm). After polishing, samples were lasered using a Nd:YVO_4 laser with a 1064 nm central wavelength, pulse duration of 15 ps, and power of 5.6W at a repetition rate of 150 kHz (Workstation from Photon Energy GmbH, Germany). Preliminary studies were made by lasering a 3x3 irradiation matrix where the laser power was changed from 10%, 40%, and 70% of the total laser power and the hatch distance (distance between consecutive laser line scans) was set to 5μm, 10μm, and 15μm.

From this matrix, the regions of highest integrated fluence (H1P700), lowest integrated fluence (H3P100), and a region in between (H2P400) were chosen to generate larger irradiated samples in order to perform further surface characterization and the corresponding biocompatilbitiy experiments.

2.2 Surface structure characterization

The resulting surfaces were characterized through scanning electron microscopy (SEM) (Auriga, Zeiss, Germany), atomic force microscopy (AFM)(Park NX20, Park Systems, South Korea), micro-Raman spectroscopy (LabRAM HR NANO Evolution, Horiba, Japan), and contact angle analysis (DSA25E, Kruss, Germany).

2.2.1 Scanning electron microscopy (SEM)

In order to obtain information on the orientation and periodicity of the generated LIPSS, 10 SEM (Auriga, Zeiss, Germany) images were taken on each lasered area. The SEM images were then analysed using the 2-dimensional Fourier Transform.[19] By doing this, it is possible to obtain the dispersion on the LIPSS orientation

angle (DLOA), which describes how *parallel* the induced structures are respect to each other. The DLOA is measured by defining the angular limits of the bright lobes on the Fourier transform, as shown in Fig.(1-B). The periodicity of the LIPSS is obtained by measuring the distance between the center of the Fourier transform to the center of the bright lobe. As it can be appreciated from Fig.(1), well defined LIPSS yield clearer lobes in the Fourier space, which result in a more precise analysis and determination of dispersion angle (A-B). The opposite occurs for more *chaotic* LIPSS, which have an equally irregular Fourier transform that makes it harder to define the bright lobes' limits (C-D).

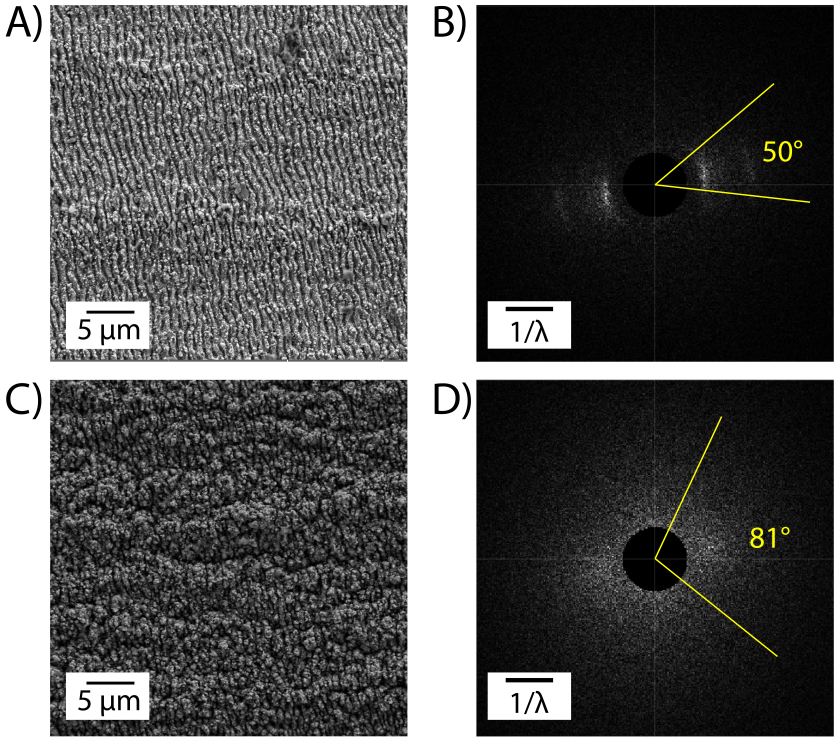

Figure 1. A) SEM image of a region irradiated using H3P100 laser parameters with its B) corresponding Fourier transform. C) SEM image of a region irradiated using H1P700 laser parameters with its D) corresponding Fourier transform. Both regions were lasered on a titanium plate polished to an initial surface roughness of 7.98nm.

2.2.2 Atomic Force Microscopy (AFM)

Average roughness and maximum peak to valley values were obtained by measuring a set of 2 20μm x 20μm AFM maps on each lasered region. The AFM system (Park NX20, Park Systems, South Korea) was equipped with an OMCL-AC160RS 10M tip, with a nominal radius of $\sim 7nm$ and a scanning speed of 0.05 Hz on non-contact mode to ensure high traceability of the surface profiles. Same methodology was followed in order to obtain the initial average roughness of the differently polished samples prior to laser treatment.

AFM measurements are of great importance as they allow for a direct correlation between the surface topography and bacterial/cell attachment values.

2.2.3 Raman spectroscopy

Raman spectra were acquired using a LabRam NANO HR800 spectrometer from Horiba Scientific in a backscattered geometry and under regular ambient conditions. A 50x long working distance objective with NA 0.55 from Leica was used, with an excitation wavelength of 532nm, a laser power of 2.6 mW, a grating of 300 lines/mm, an integration time of 1s and 2 accumulations per point. To obtain statistically significant mean spectra, a set of 3, 50x50 point maps were measured on each lasered region for a total of 7,500 measured points.

2.2.4 Contact angle (CA) measurements

After initial surface characterization, a set of larger lasered samples was generated under the same conditions in order to obtain CA measurements. Before measuring the CA, samples were submerged in acetone (99.5 %, Höfer chemie GmbH) and placed under ultrasonic bath for 10 min, to then go into a second 10 min ultrasonic bath under isopropanol (99.9 %, Höfer chemie GmbH). Five drops of $2\mu l$ ultrapure water were deposited on each surface to obtain the reported CA value.

2.3 Cytocompatibility and antibacterial activity

2.3.1 Cell culture

Cytocompatibility of Titanium and stainless steel surfaces was evaluated by culturing with pre-osteoblastic MG63 cells (ATCC) for 5 days. Cells were maintained in alpha-minimum essential medium (α-MEM) supplemented with 10% (v/v) fetal bovine serum (FBS), penicillin (100 IU/mL), streptomycin (100 μg/mL) and amphotericin B (2.5 μg/mL; Gibco) with regular media change (every 2 days). Prior to seeding, all metal plates were sterilized with 70% ethanol (30 mins) followed by UV treatment (30 mins). They were subsequently seeded at a density of $2x10^4$ cells/cm^2 in a 24 well plate and incubated at 37 °C, 95% humidity and 5% CO2 atmosphere. Laser modified titanium and stainless steel were subsequently assessed for proliferation (Resazurin assay), morphology (Scanning electron microscopy) and osteogenic potential (Alkaline phosphatase activity).

2.3.2 Resazurin assay

Resazurin based fluorescent assay was used to monitor the viability and proliferation of MG63 cells cultured over Titanium and stainless steel surfaces after 1, 3 and 5 days of cell seeding. The seeded metal plates were transferred to a fresh 24 well plate before incubating them with medium supplemented with 10% Resazurin solution (Sigma) for 3 hours at 37 °C in CO2 incubator. Fluorescent intensity of the reduced, fluorescent product formed by metabolically active cells (Resorufin) was measured at 530/570nm (Excitation/emission) in a microplate reader (Synergy HT, Biotek). All measurements were expressed at relative fluorescent units (RFU).

2.3.3 Alkaline Phosphatase (ALP) activity

Alkaline phosphatase (ALP) activity of cells cultured over metal plates was measured to evaluate the osteoblastic or bone formation potential of the various laser modified surfaces. Cells seeded over titanium and stainless steel were washed with 1X PBS and lysed with 0.1% triton-X-100 (30 mins) after 5 days of culture. The cell lysate with ALP enzyme was incubated with 25mM p-nitrophenyl phosphate substrate (Sigma-Aldrich) for 1 hour at 37 °C in CO2 incubator. The enzymatic reaction was stopped with 5M NaOH. The hydrolysed product (para-nitrophenol) was measured (λ_{max}=400 nm) a microplate reader. The ALP Activity was normalized to total protein content, which was measured using DCTM protein assay (Biorad) as per manufacturer's instructions.

2.3.4 SEM

The morphology and attachment of cells on various surface modifications were analyzed by SEM. All seeded samples were fixed in 1.5% glutaraldehyde solution prepared in 25% cacodylate solution (TAAB laboratories) for 30 minutes. They were dehydrated in graded ethanol concentrations (50%, 70%, 90%, 100% ethanol) followed by critical point drying and spur-coating with gold-palladium. Imaging was performed with Scanning electron microscope (JEOL JSM-700).

2.3.5 Antibacterial activity

Antibacterial activity of laser modified Titanium and stainless steel was assessed against a gram positive bacteria, *Staphylococcus aureus* (ATCC 25923) and a gram negative bacteria, Escherichia coli (ATCC 25922). Samples were incubated with 104 CFU/ml of bacteria in logarithmic growth phase in Tryptic Soy Broth (TSB) medium (Liofilchem) in a shaker incubator for 24hrs at 37°C. Viability of both planktonic (non-adherent population in suspension) and sessile (adherent population on surface) bacteria was measured after 24 hours of culture using 10% Resazurin solution (prepared in TSB). The bacterial suspension with planktonic bacteria was incubated with Resazurin solution for 10 minutes while sessile bacteria were incubated for 1 hour after washing thrice with saline and transferring to fresh plate. Fluorescent intensity was measured as described before. Additionally, absorbance at 600nm was measured for the bacterial suspension (not shown). Samples were prepared for SEM imaging (as described before) to assess potential for biofilm inhibition.

3. RESULTS

3.1 Roughness

Table(1) shows the average roughness (Ra) values for the differently polished samples of titanium and stainless steel. As expected, Ra decreases with increasing polishing steps. A similar trend is observed for peak to valley (Rz) values. This trend is clearly visible in Fig.(2), where $20\mu m$ x $20\mu m$ AFM images of the differently polished samples for both titanium and stainless steel are compared.

In row A (polishing grain size = $18.3\mu m$) clear scratches from the machining of the samples are visible. The line profile shows a peak to valley difference close to $1\mu m$ for titanium, while for stainless steel the difference is approximately $400nm$. However, the stainless steel sample shows more scratches (with lower peak to valley variations) compared to its titanium counterpart, which shows more debris on the surface. Row B (polishing grain size = $8.4\mu m$) line profiles show a decrement in the roughness values compared to row A for both the materials and, particularly for stainless steel, big debris are removed from the surface, leaving behind the previously observed scratches and even lower peak to valley values (from $Rz = 1,339nm$ to $Rz = 693nm$). It is important to notice the huge difference in Ra values for stainless steel from row A to row B, which can also be appreciated in Table(1). A similar very remarked discontinuity in the Ra values is observed for titanium on the following polishing step, row C (polishing grain size = $5\mu m$), where relatively large debris are not predominant anymore, leaving a surface with low deepness scratches. In the case of stainless steel, machining scratches are still visible at row C, but with lower Ra and Rz values compared to those for row B.

In row D (polishing grain size $0.5\mu m$), both surfaces present a generally smooth area, with machining scratches barely visible, yielding Ra values of $5nm$ and $2nm$ for titanium and stainless steel, respectively. Some small dirt particles are present on measured maps but have no significant impact on the averaged values.

Table 1. Average roughness titanium and stainless steel polished samples before laser treatment. Reported values of Ra and Rz are in nm.

Polishing grain size		$18.3\mu m$	$8.4\mu m$	$5\mu m$	$0.5\mu m$
Titanium	Ra	81.4 ± 0.8	74.7 ± 0.8	10.6 ± 0.2	5.3 ± 0.1
	Rz	1338.9 ± 136	693.1 ± 110	138.8 ± 17	197.5 ± 35.9
Stainless Steel	Ra	92.7 ± 8	17.7 ± 1	6.8 ± 1	2.0 ± 0.1
	Rz	619.7 ± 43	163.9 ± 12	130.4 ± 54	73.2 ± 4.8

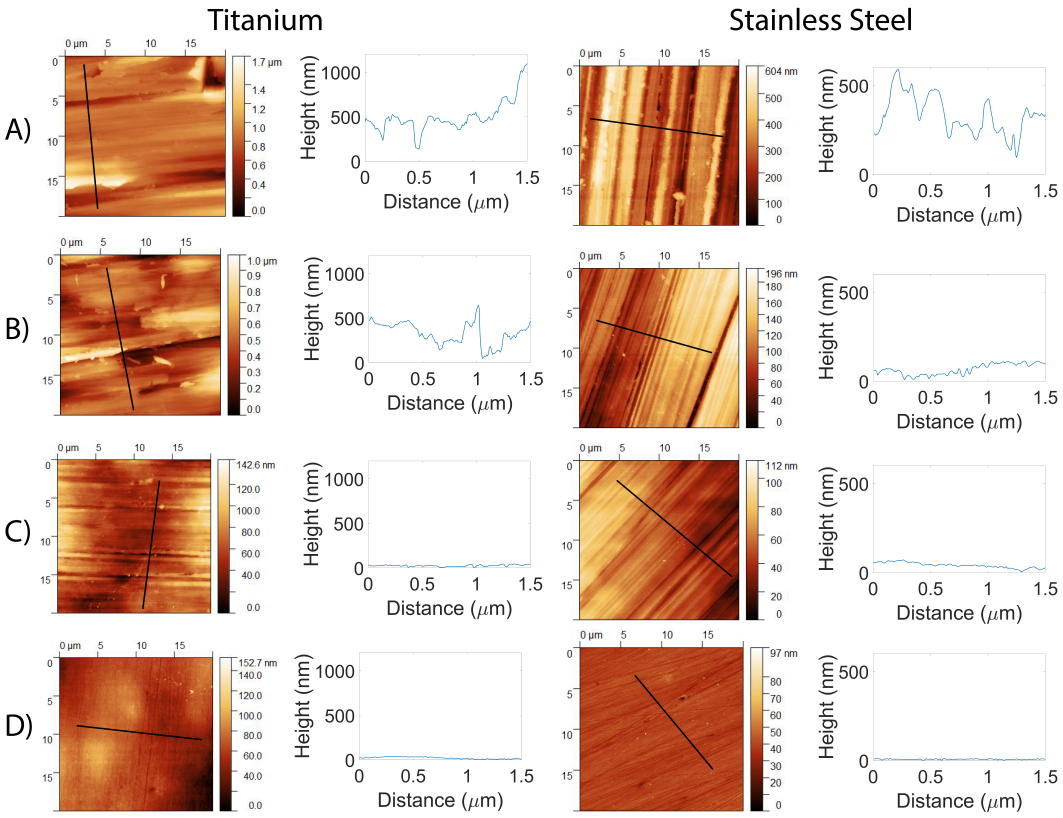

Figure 2. Representative AFM maps of $20\mu m$ x $20\mu m$ measured on samples polished with A) $18.3\mu m$, B) $8.4\mu m$, C) $5\mu m$, and D) $0.5\mu m$ polishing grain sizes. Black lines indicate the cross section lines extracted, which can be seen on the right of the AFM image. The height scale has been selected to be always the same for each material in order to better compare the different values.

Samples were lasered after being polished as described in the materials and methods section. A 3x3 irradiation matrix was lasered by changing the laser power and the hatch distance. The average roughness (Ra) values for the previously selected regions of interest (H1P700, H2P400, H3P100) were measured and are shown in Fig.(3) for both titanium and stainless steel. The first major difference standing out between the two materials regards the large variation in Ra values that stainless steel shows for samples with a high initial Ra. In the case of stainless steel, for high integrated fluence values, Ra values of lasered regions decreases with a decreasing initial Ra, while the opposite seems to happen for low integrated fluence values, where the lowest Ra is measured at samples polished with an $18.3\mu m$ polishing grain size. Samples lasered with H2P400 conditions show a similar trend as those irradiated with H1P700, with Ra values decreasing with increasing polishing steps.

Titanium regions irradiated with H1P700, and H2P400 conditions present a minimum Ra for a polishing step obtained using a grain size of $8.4\mu m$, and higher Ra values increasing the polishing steps. The opposite is observed for regions irradiated with H3P100 parameters, where the lowest Ra values appear for samples polished with a grain size of $5nm$ and $0.5nm$, while the highest Ra value are associated to samples polished with a grain size of $8.4\mu m$. In general, roughness values measured for titanium vary less, with the highest difference being $40nm$, with respect to the roughness for stainless steel, where the difference between the highest (H1P700) and the lowest value (H3P100) is $486nm$.

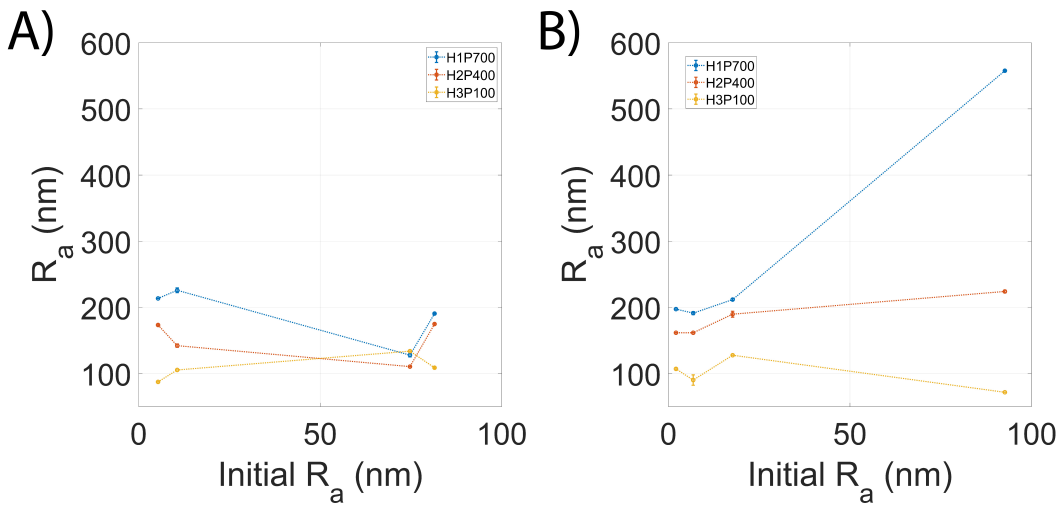

Figure 3. Ra values for lasered regions on differently polished samples of A) titanium and B) stainless steel. Scale bars were chosen to be the same to better compare results between materials.(H1P700 = blue, H2P400 = orange, H3P100 = yellow)

3.2 Periodicity and orientation

Calculated DLOA values for titanium and stainless steel are shown in Fig.(4) and Fig.(5), respectively. The DLOA values for titanium tend to vary less for regions lasered with a hatch distance of $10\mu m$, having the DLOA value converge for all differently lasered regions on high polished samples. In the case of hatch value of $H = 15\mu m$, experimental values differ more between each laser power condition, however, DLOA values also tend to converge at highly polished regions regardless of the laser irradiation intensity. The lowest DLOA values in this case are obtained for the lowest lasering power. For a hatch distance of $H = 5\mu m$, DLOA values tend to converge in the opposite direction (for higher initial Ra surfaces). It is important to note that the lowest value shown here (H1P700), does represent one of the *worst case scenario* for analysis shown in Fig.(1-C,D), this might explain the sudden drop in the calculated DLOA (45.54°). Therefore, even if the uncertainty for this experimental point is low (analysis performed averaging 10 SEM images), our values might be precise, but not accurate.

We can also see an expected trend if we compare Fig.(3) and Fig.(4), as higher DLOA values (less organized structures) lead to a higher Ra of the lasered surface.

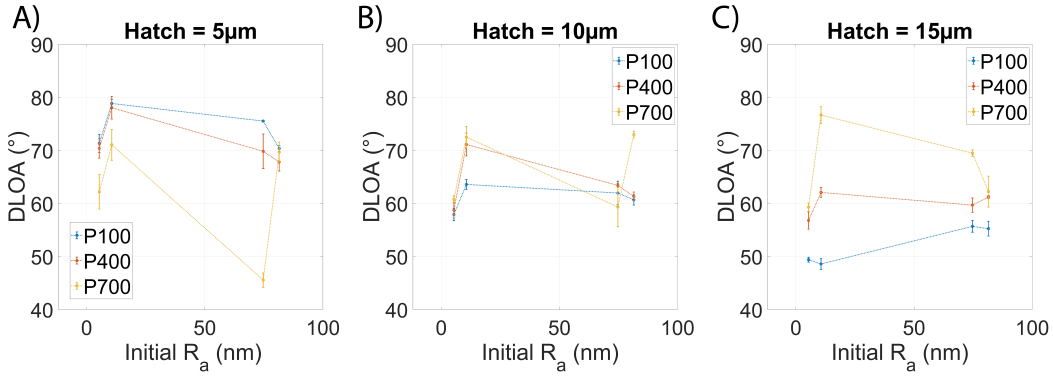

Figure 4. DLOA of regions 3, 5, and 7 of the irradiation matrix on titanium for different hatch distances and differently polished samples.

In the case of stainless steel, for $H = 5\mu m$, DLOA values tend to converge in highly polished samples, opposite to titanium. However, a minimum is encountered for all laser power levels at samples polished with a polishing grain size of $8.4\mu m$. Regions irradiated with $H = 10\mu m$ highlight that DLOA values increase with increasing laser power, with a big gap between P100 and P400/P700 lasering conditions. Regions irradiated with P400 and P700 conditions show minimum DLOA values for surfaces polished with a grain size of $8.4\mu m$, while this minimum is shifted to surfaces polished with a grain size of $5\mu m$ for regions irradiated at P100. For a hatch distance of $H = 15\mu m$, all lasering conditions result on a minimum DLOA when surfaces are polished with a grain size of $18.3\mu m$, while converging to similar values at surfaces polished with a grain size of $8.4\mu m$

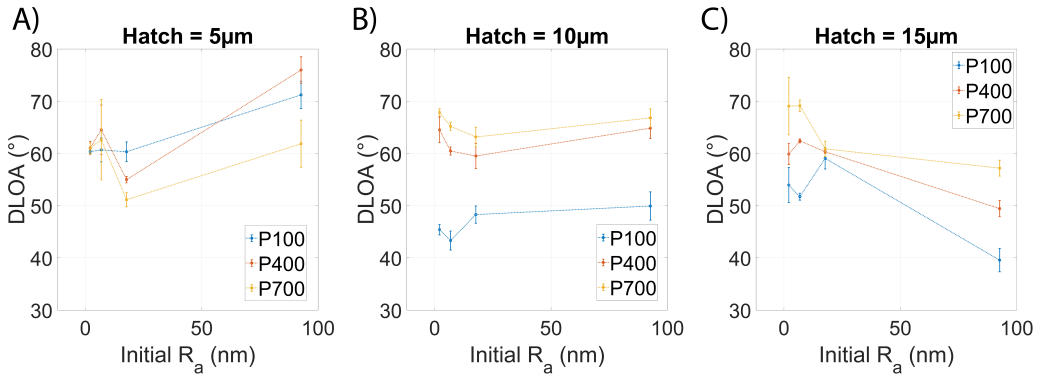

Figure 5. DLOA of regions 3, 5, and 7 of the irradiation matrix on stainless steel for different hatch distances and differently polished samples.

Period values for titanium and stainless steel are shown in Fig.(6) and Fig.(7). In the case of titanium, it is observed that periods are larger for the highest laser power at $H = 5\mu m$, which is reversed for $H = 15\mu m$, where the regions lasered with the lowest laser power show the highest periodicity values. This is also true for $H = 10\mu m$. However, in this case the periodicity does not seem to be greatly affected by the initial surface roughness of the samples in any of the laser power cases. Periodicity shows to have a higher dependency on the initial surface roughness for lower hatch distances.

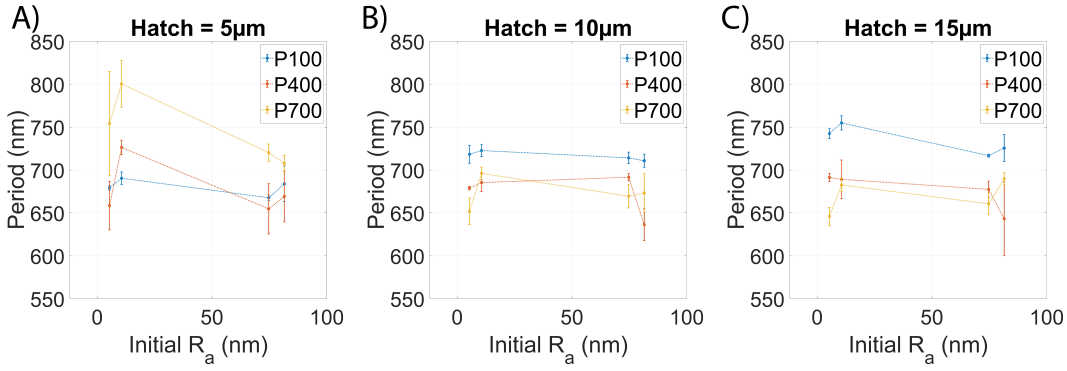

Figure 6. Period of regions 3, 5, and 7 of the irradiation matrix on titanium for different hatch distances and differently polished samples.

Stainless steel periodicity values for $H = 5\mu m$ converge on surfaces polished with a grain size of $18.3\mu m$, and decrease as the polishing steps increase for P400 and P700. This is not true for the lowest laser power (P100), where the minimum periodicity value occurs at samples polished with a grain size of $8.4\mu m$, to then rise again by $\sim 40nm$ for the following polished steps. In the case of $H = 10\mu m$, the lowest laser power (P100) yields

higher structure periods, while P400 and P700 conditions share similar results. Regions lasered with $H = 15\mu m$ show an interesting behaviour as there is a large difference on LIPSS periodicity for P100, compared to P400 and P700, with P100 structures showing the largest periodicity values.

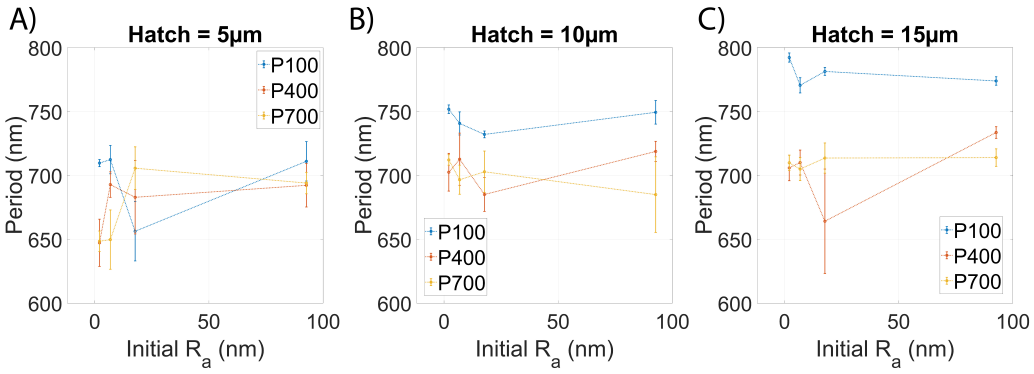

Figure 7. Period of regions 3, 5, and 7 of the irradiation matrix on stainless steel for different hatch distances and differently polished samples.

In the case of stainless steel, it is easier to observe that the periodicity values tend to increase with increasing hatch. This can be explained by a reinforced feedback process LIPSS formation go through. Lower hatch distances means a higher overlap between consecutive scans. This means that after LIPSS are formed, consecutive scans interact with an already periodic structure, this leads to higher focus of the electric field and a reduction on the LIPSS periodicity.

3.3 Contact Angle

Contact angle values for titanium and stainless steel are reported in Fig.(8), as well as a picture showing the lateral view of the measuring system in the case of the maximum and minimum values recorded for each material. For titanium, CA values do not show a strong relation to the initial surface roughness. Regions lasered with H1P700 and H2P400 show a slight increase in CA values as the polishing steps increase, from 29° to 36° and from 27° to 43° respectively. The opposite occurs for H3P100, where the highes CA value (44°) appears for the least polished sample, and the minimum CA value (34°) corresponds to the sample polished with a grain size of $0.5\mu m$.

Stainless steel CA values show, instead, a higher dependence on the initial surface roughness values, with regions polished with a larger grain size ($18.3\mu m$) showing lower CA values for all laser powers. As the polishing steps increase, so does the CA, having a maximum ($\sim 104°$) at samples polished with a grain size of $5\mu m$ to then decrease again by approximately 10% for the following polishing step. This is of great importance as this can allow to tailor CA values by changing the polishing steps, while maintaining the laser parameters.

Stainless steel samples can be tailored between hydrophobic and hydrophilic by changing the initial surface roughness and maintaining the lasering conditions, with a maximum CA difference of $\sim 100°$ as it is shown on Fig.(8). In the case of titanium, CA values are mostly maintained through the different polishing steps, allocating the modified surfaces in the hydrophilic regime.

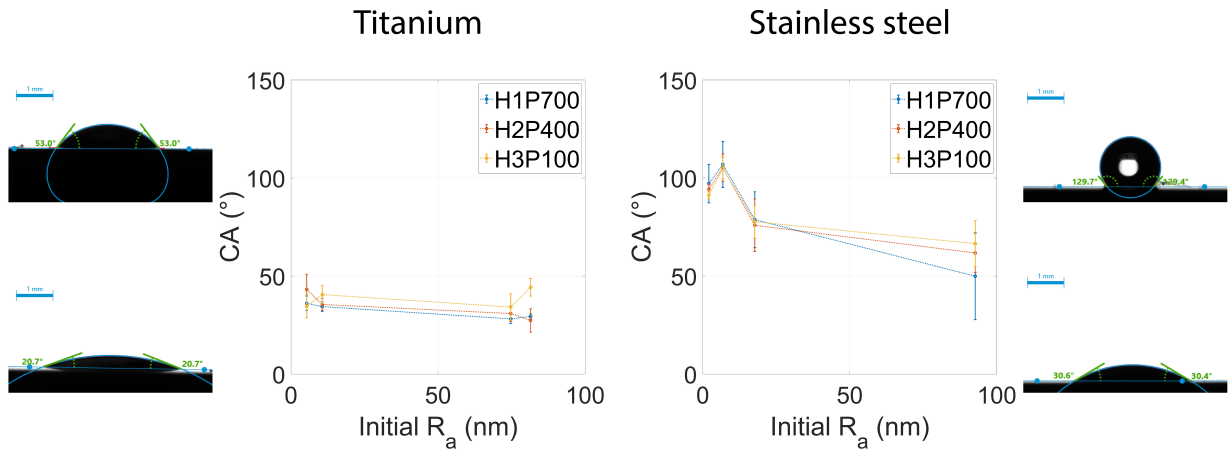

Figure 8. Contact Angle (CA) values for H1P700, H2P400, and H3P100 lasered regions on differently polished samples for both titanium and stainless steel. Side panels show an image of the highest (top) and lowest (bottom) values recorded for each material.

3.4 Raman spectroscopy

Mean Raman spectra for titanium samples are reported in Fig.(9). The first general remark that can be made which involves all the spectra is that only a broad peak is observed for samples irradiated at the lowest integrated fluence (H3P100). However, when increasing the deposited energy (H2P400) peaks start to appear on the different spectra for every polishing step. For regions irradiated with the highest total fluence (H1P700) peaks get clearly defined at $150cm^{-1}$, $236cm^{-1}$, $440cm^{-1}$, and $589cm^{-1}$, which correspond to TiO_2 rutile phase.[20] The power dependency of the spectra indicates that oxidation is enhanced by the laser irradiation.

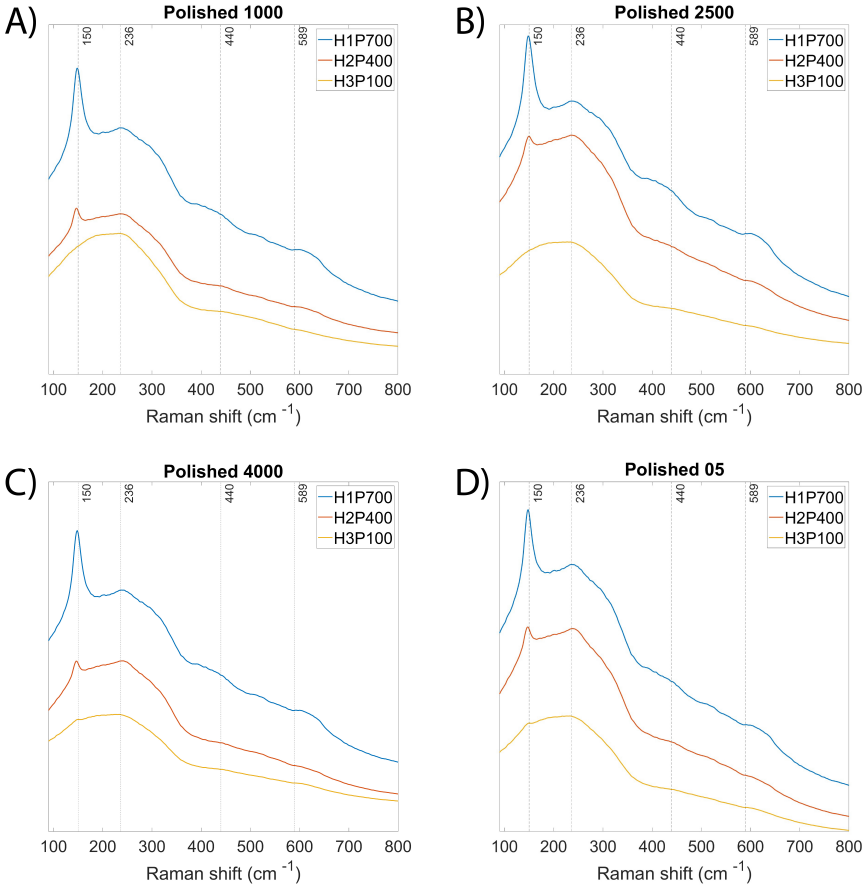

Figure 9. Raman spectra of regions irradiated with H1P700 (blue), H2P400 (orange), and H3P100 (yellow) lasering conditions, on samples polished with a grain size of A) 18.3μm, B) 8.4μm, C) 5μm, and D) 0.5μm on titanium. Vertical axis shows intensity in arbitrary units.

In the case of stainless steel, Fig.(10), mean Raman spectra shows a broad peak at 690cm^{-1} for all lasering conditions, which is attributed to a stainless steel spinel oxide phase.[21] Regions irradiated with the lowest laser intensity (H3P100) show no other clear peak. When increasing the laser power (H2P400), peaks at 350cm^{-1} and 528cm^{-1}, attributed to Cr_2O_3,[22] tend to get more defined, being more clear for regions irradiated with the highest laser power (H1P700). Broad peaks show the presence of amorphous oxide generation, while the laser power dependence of the generated peaks shows again, a clear trend for laser induced oxidation.

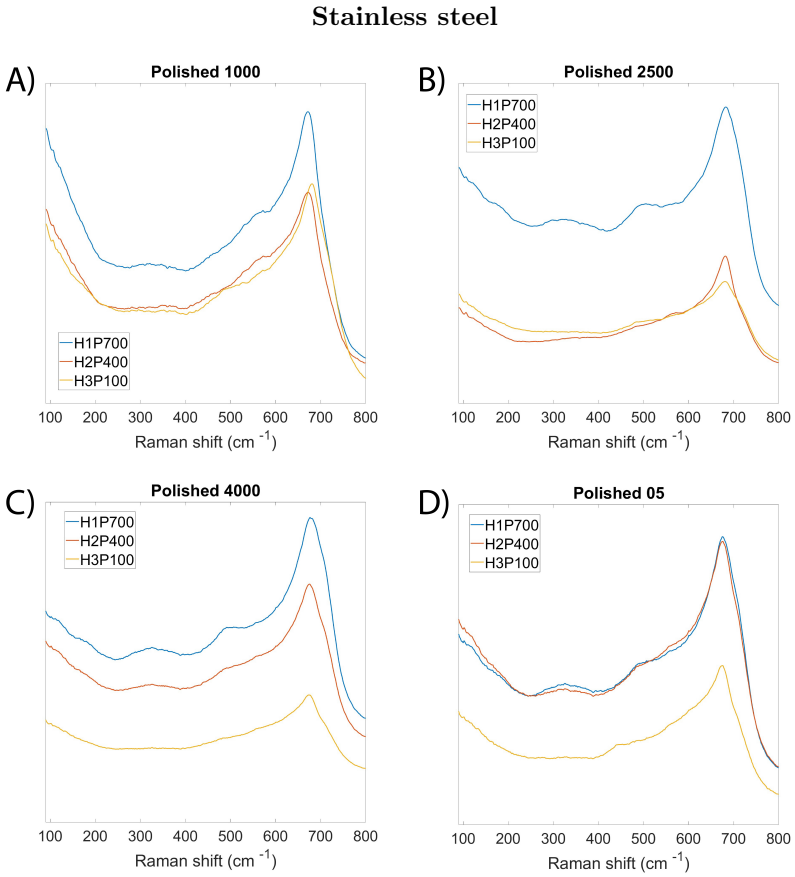

Figure 10. Raman spectra of regions irradiated with H1P700 (blue), H2P400 (orange), and H3P100 (yellow) lasering conditions, on samples polished with a grain size of A) 18.3μm, B) 8.4μm, C) 5μm, and D) 0.5μm on stainless steel. Vertical axis shows intensity in arbitrary units.

3.5 Cytocompatibility assessment

Cytocompatibility of laser treated titanium and stainless steel surfaces was assessed using pre-osteoblastic MG63 cells. Unlasered surfaces of titanium and stainless steel were used as respective controls. Cell proliferation was measured at Day 1 and Day 5 of cell culture. All laser treated titanium surfaces showed similar cell proliferation and total protein content at both time points, with increased proliferation at Day 5. However, ALP activity (normalized to total protein content) for polished titanium surfaces showed an increasing trend from H3P100 to H1P700 modification. Stainless steel surfaces, on the other hand, showed a different proliferation trend. Even though a decrease in the cell proliferation was observed for both unpolished and polished laser treated surfaces, the ALP activity of unpolished was not significantly different between all modifications. Further, an increase in osteogenic activity was observed for polished stainless steel from H3P100 to H1P700 modifications (Fig.(11)). These results were supported by SEM images at Day 3 of culture. Cytocompatibility with both titanium and stainless steel is evident at high magnification SEM images, demonstrated by thin, needle-like protrusions of lamellipodia and filopodia, extending towards the nanotopographical structures on the surface (Fig.(12)).

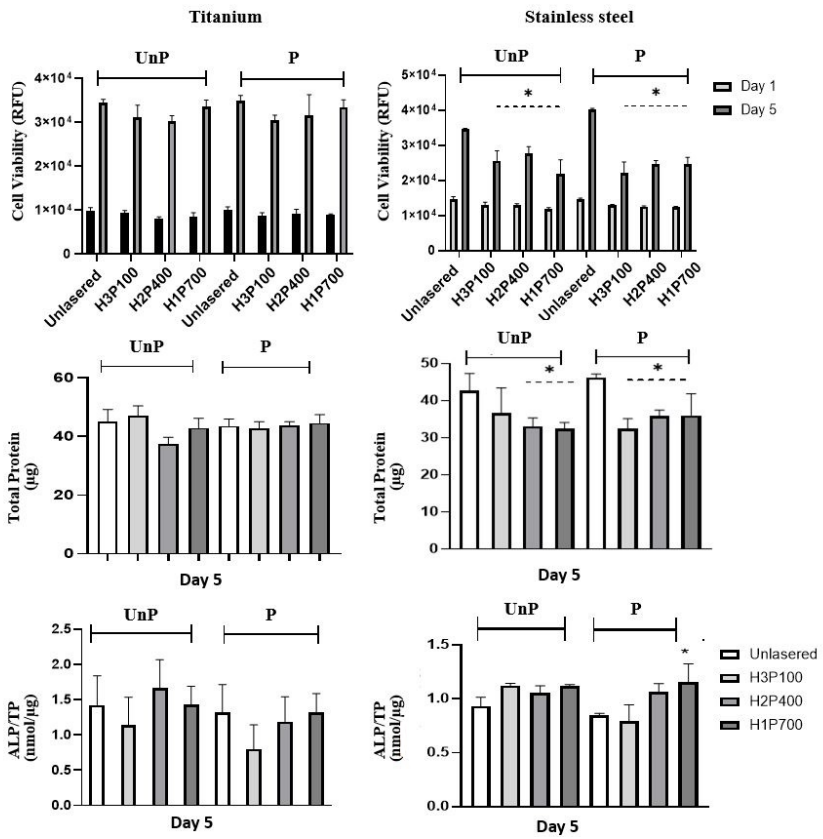

Figure 11. Behaviour of MG63 osteoblastic cells cultured over unlasered and lasered Titanium and Stainless steel surfaces, unpolished (UnP) and polished (P). Cell viability, total protein content and alkaline phosphatase (ALP) activity. *Statistically significant different from unlasered surfaces.

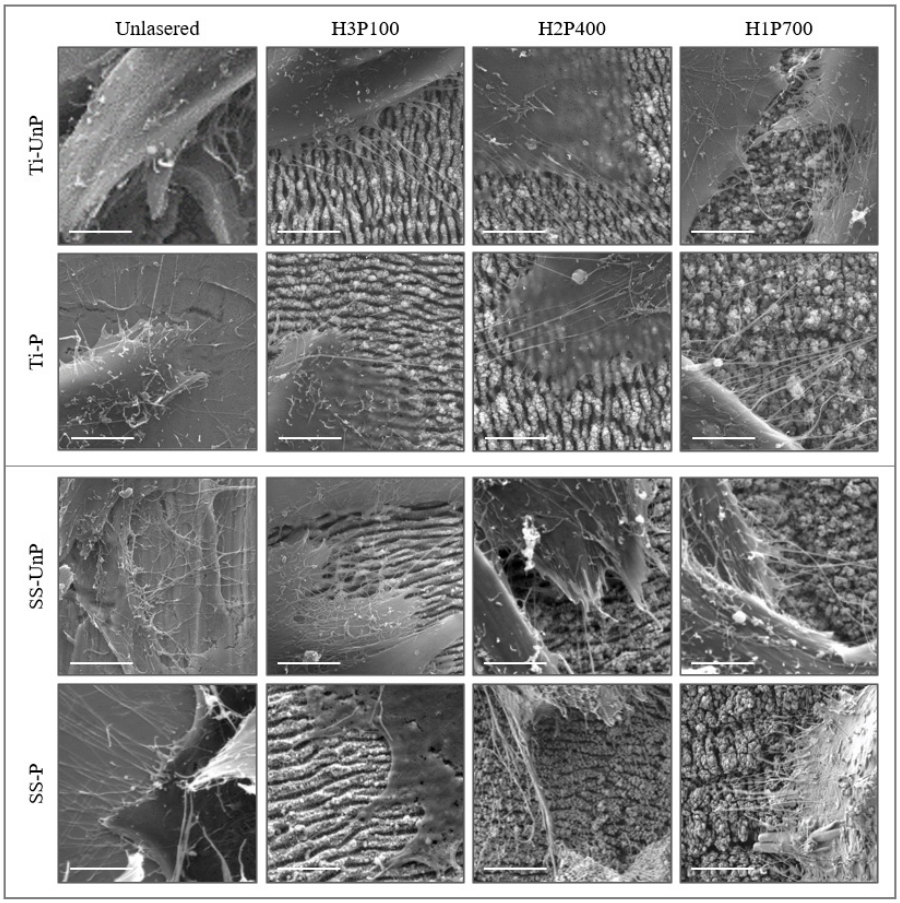

Figure 12. Representative high magnification SEM images of MG63 osteoblastic cells cultured over unlasered and lasered Titanium (Ti) and Stainless steel (SS) surfaces, unpolished (UnP) and polished (P) (Scale bar = 5 μm).

3.6 Antibacterial activity

Antibacterial behavior of laser modified titanium and stainless steel was analyzed using *Staphylococcus aureus* (Gram positive bacteria) and *Escherichia coli* (gram negative bacteria). Bacterial viability was measured for planktonic populations (bacteria in suspension) and sessile bacteria (bacteria adhered to the surface) using unlasered surfaces as controls. There was a tendency for decreased viability of *E.coli* (for both planktonic and sessile populations) on laser treated Titanium surfaces compared to unlasered controls. For *S. aureus*, only planktonic population showed reduced viability. These results were in concordance with SEM images. We observed a healthy bacterial morphology for *S. aureus* (round and smooth membrane) and *E. coli* (rod shaped and round) on unlasered surfaces Fig.(13). Laser treated surfaces induced severe damage to bacterial cell membrane, as seen from the rough, collapsed morphology. There were also anomalies in the cell division process, represented by long unseparated, chains of bacteria. They were clearly prevented from forming a biofilm on laser treated surfaces as observed by a visibly reduced bacterial population with individual bacteria. For stainless steel, even though no significant reduction in viability of *E. coli* and *S. aureus* was found, we observed clear signs of bacterial damage on laser treated surfaces after 24 hours of culture (Fig.(14)).

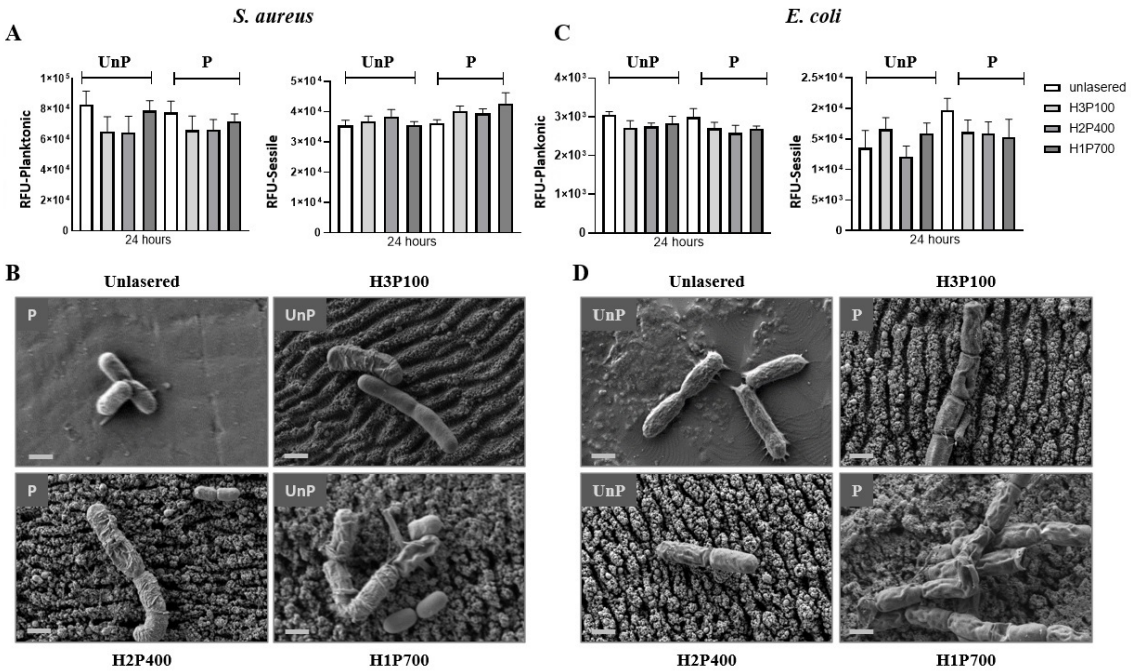

Figure 13. Antibacterial activity of Titanium surfaces - unpolished (UnP) and polished (P), non-treated and laser-treated (H3P100, H2P400, H1P700). A and C: Viability (RFUs) of planktonic and sessile *S. aureus* and *E. coli*, respectively; B and D: Representative high magnification SEM images of the morphology of *S. aureus* and *E. coli* on different Titanium surfaces (Scale bar = 1 μm).

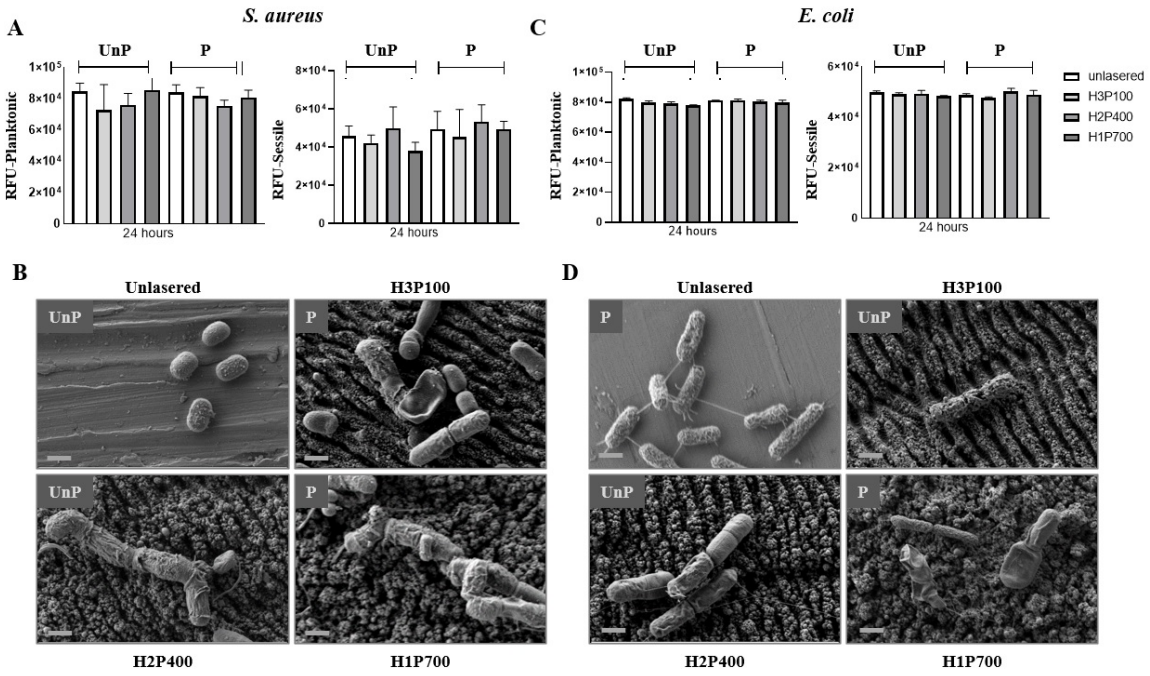

Figure 14. Antibacterial activity of Stainless steel surfaces - unpolished (UnP) and polished (P), non-treated and laser-treated (H3P100, H2P400, H1P700). A and C: Viability (RFUs) of planktonic and sessile *S. aureus* and *E. coli*, respectively; B and D: Representative high magnification SEM images of the morphology of *S. aureus* and *E. coli* on different Stainless steel surfaces (Scale bar = 1 μm).

4. DISCUSSION

As previously mentioned in the introduction, titanium and stainless steel are among the most used materials for high stress bearing implants,[1] however, their difference in elastic modulus[5] makes their processing intrinsically different. From the very beginning, different mechanical behaviors as a function of the polishing steps are seen, with titanium being rougher and requiring more polishing steps than stainless steel in order to significantly reduce the average roughness of the surface to be treated.

Titanium and stainless steel also have different thermal properties,[23,24] which directly affect the laser processing as heat is differently distributed among both materials. This is stressed in the presented Ra values of laser treated regions (Fig.(3)), where titanium values, although dependent on the initial Ra of the surface, vary less in comparison with the final Ra values of laser treated regions in stainless steel. The LIPSS orientation values have a similar trend for both materials, with increasing DLOA values for lower hatch distances and with more consistent DLOA values for regions treated with a hatch distance of $H = 10\mu m$. It can also be noted that for both materials, the lower processing power (P100), yields both the highest DLOA (H1P100) and the lowest DLOA (H3P100), meaning that processing at lower laser powers allows for a better control of the final structure by tailoring the remaining parameters (like hatch distance and initial surface roughness).

Periodicity has a lower dependency on the initial Ra than the DLOA values, and shows opposite behaviors for titanium and stainless steel. In specific, while values for titanium tend to decrease with increasing hatch distance, stainless steel values are higher for higher hatch values. However, comparing these trends to the measured Ra values of laser treated regions, both materials show that Ra and periodicity are directly correlated. This is an important relation to follow as it allows not only to tailor the period of the required structure, but also the deepness between the formed trenches. For CA values, both materials present a dependence on the initial surface roughness, with stainless steel data showing a higher variation between the differently polished samples.

Our study also demonstrates that generation of LIPSS structures results in antibacterial properties on bone compatible surfaces without affecting their cytocompatibility. This is also in concordance with reported antimicrobial studies on LIPSS generation on metallic surfaces.[25] The laser modified titanium surfaces supported

better cell proliferation compared to stainless steel. Further, the osteogenic potential was unaffected on unpolished surfaces while polished surfaces showed enhanced osteogenic effect upon laser induction (highest for H1P700 modification). Two key parameters influencing cytocompatibility are surface wettability and surface roughness.[26] LIPSS-induced nano-topographies improve overall wettability, with H1P700 laser modification showing highest wettability. Moreover, surface roughness is reduced upon polishing the surfaces but is recovered with laser treatment to improve cellular attachment. Additionally, a pattern for reduction of bacterial viability on both titanium and stainless steel is evident, while it does not appear significant, possibly due to metabolically quiescent bacteria and bacteriostatic effect. However, SEM images showed severe damages to bacterial morphology along with significantly reduced bacterial adhesion and colonization. LIPSS structures induced rupture and bursting of the bacterial membrane. Moreover, the reduction in viability is more prominent in *S. aureus*, which is more clinically relevant to bone infections. These differences can be explained by the differences in shape and size of *S. aureus* (0.5 to 1 μm) and *E. coli* (1 to 2 μm). Generation of nano-scaled topographies reduces the surface area for attachment as the size of periodicities is much smaller than bacterial dimensions. Due to the elongated and relatively larger size of *E. coli*, they encounter even lesser contact points for attachment.[27] These results are also supported by studies of laser induced nanostructuring on different material types[28,29] demonstrating reduced bacterial attachment on laser treated surfaces.

5. CONCLUSIONS

We have shown that the initial surface roughness of stainless steel and titanium surfaces plays a different role on the resulting generated structures, with stainless steel being highly tunable and showing larger differences in final roughness, periodicity of the generated structures, and surface wettability according to the initial polishing steps. This gives stainless steel the advantage of being tailored between hydrophilic (50°) and hydrophobic (100°), which directly impacts how the surface interacts with the medium it is implanted in. Even though titanium shows a lower dependency on initial surface roughness, antibacterial results show lower bacterial proliferation for all lasered surfaces. This might be attributed on the different chemistry of the generated oxide layers for both materials. Generally, both structured materials show to be a a proper medium for cell proliferation, and increasing the initial polishing steps allows for a more controlled surface structuring, while also avoiding large surface cracks where bacteria could allocate and proliferate.

REFERENCES

[1] Saini, M., Singh, Y., Arora, P., Arora, V., and Jain, K., "Implant biomaterials: A comprehensive review," *World Journal of Clinical Cases: WJCC* **3**(1), 52 (2015).

[2] Elias, C., Lima, J., Valiev, R., and Meyers, M., "Biomedical applications of titanium and its alloys," *Jom* **60**(3), 46–49 (2008).

[3] Bothe, R., "Reaction of bone to multiple metallic implants," *Surg Gynecol Obstet* **71**, 598–602 (1940).

[4] Sidambe, A. T., "Biocompatibility of advanced manufactured titanium implants—a review," *Materials* **7**(12), 8168–8188 (2014).

[5] Ratner, B. D., Hoffman, A. S., Schoen, F. J., and Lemons, J. E., "Biomaterials science: an introduction to materials in medicine," *San Diego, California* , 162–4 (2004).

[6] Van Noort, R., "Titanium: the implant material of today," *Journal of Materials Science* **22**(11), 3801–3811 (1987).

[7] Solar, R. J., Pollack, S. R., and Korostoff, E., "In vitro corrosion testing of titanium surgical implant alloys: an approach to understanding titanium release from implants," *Journal of Biomedical Materials Research* **13**(2), 217–250 (1979).

[8] Pan, J., Leygraf, C., Thierry, D., and Ektessabi, A., "Corrosion resistance for biomaterial applications of tio2 films deposited on titanium and stainless steel by ion-beam-assisted sputtering," *Journal of Biomedical Materials Research: An Official Journal of The Society for Biomaterials and The Japanese Society for Biomaterials* **35**(3), 309–318 (1997).

[9] Modaresifar, K., Azizian, S., Ganjian, M., Fratila-Apachitei, L. E., and Zadpoor, A. A., "Bactericidal effects of nanopatterns: A systematic review," *Acta biomaterialia* **83**, 29–36 (2019).

[10] Linklater, D. P., Baulin, V. A., Juodkazis, S., Crawford, R. J., Stoodley, P., and Ivanova, E. P., "Mechano-bactericidal actions of nanostructured surfaces," *Nature Reviews Microbiology* **19**(1), 8–22 (2021).

[11] Siddiquie, R. Y., Gaddam, A., Agrawal, A., Dimov, S. S., and Joshi, S. S., "Anti-biofouling properties of femtosecond laser-induced submicron topographies on elastomeric surfaces," *Langmuir* **36**(19), 5349–5358 (2020).

[12] Bonse, J., Höhm, S., Kirner, S. V., Rosenfeld, A., and Krüger, J., "Laser-induced periodic surface structures—a scientific evergreen," *IEEE Journal of selected topics in quantum electronics* **23**(3) (2016).

[13] Stratakis, E., Bonse, J., Heitz, J., Siegel, J., Tsibidis, G., Skoulas, E., Papadopoulos, A., Mimidis, A., Joel, A.-C., Comanns, P., et al., "Laser engineering of biomimetic surfaces," *Materials Science and Engineering: R: Reports* **141**, 100562 (2020).

[14] Dostovalov, A. V., Derrien, T. J.-Y., Lizunov, S. A., Přeučil, F., Okotrub, K. A., Mocek, T., Korolkov, V. P., Babin, S. A., and Bulgakova, N. M., "Lipss on thin metallic films: New insights from multiplicity of laser-excited electromagnetic modes and efficiency of metal oxidation," *Applied Surface Science* **491**, 650–658 (2019).

[15] Segovia-Olvera, P., Sotelo, L., Esqueda-Barron, Y., Plata, M., Ramos, N., and Camacho-Lopez, S., "Femtosecond large-area fabrication of multi-phase titanium oxide lipss on thin films," *Applied Surface Science* **606**, 154762 (2022).

[16] Saadatian-Elahi, M., Teyssou, R., and Vanhems, P., "Staphylococcus aureus, the major pathogen in orthopaedic and cardiac surgical site infections: a literature review," *International Journal of Surgery* **6**(3), 238–245 (2008).

[17] Hudson, M. C., Ramp, W. K., and Frankenburg, K. P., "Staphylococcus aureus adhesion to bone matrix and bone-associated biomaterials," *FEMS microbiology letters* **173**(2), 279–284 (1999).

[18] Lu, Y., Cai, W.-j., Ren, Z., and Han, P., "The role of staphylococcal biofilm on the surface of implants in orthopedic infection," *Microorganisms* **10**(10), 1909 (2022).

[19] Bonse, J., Kirner, S. V., and Krüger, J., "Laser-induced periodic surface structures (lipss)," *Handbook of laser micro-and nano-engineering* , 1–59 (2020).

[20] Arsov, L. D., Kormann, C., and Plieth, W., "Electrochemical synthesis and in situ raman spectroscopy of thin films of titanium dioxide," *Journal of Raman spectroscopy* **22**(10), 573–575 (1991).

[21] Srisrual, A., Coindeau, S., Galerie, A., Petit, J.-P., and Wouters, Y., "Identification by photoelectrochemistry of oxide phases grown during the initial stages of thermal oxidation of aisi 441 ferritic stainless steel in air or in water vapour," *Corrosion Science* **51**(3), 562–568 (2009).

[22] Chen, Z., Wang, L., Yu, Z., Li, F., Sun, Z., Zhao, H., and Chou, K. C., "Corrosion process of stainless steel 441 with heated steam at 1,000° c," *High Temperature Materials and Processes* **36**(7), 717–724 (2017).

[23] Kim, C. S., "Thermophysical properties of stainless steels," tech. rep., Argonne National Lab., Ill.(USA) (1975).

[24] Valencia, J. J. and Quested, P. N., "Thermophysical properties," (2013).

[25] Du, C., Wang, C., Zhang, T., and Zheng, L., "Antibacterial performance of zr-bmg, stainless steel, and titanium alloy with laser-induced periodic surface structures," *ACS Applied Bio Materials* **5**(1), 272–284 (2021).

[26] Song, F., Koo, H., and Ren, D., "Effects of material properties on bacterial adhesion and biofilm formation," *Journal of dental research* **94**(8), 1027–1034 (2015).

[27] Epperlein, N., Menzel, F., Schwibbert, K., Koter, R., Bonse, J., Sameith, J., Krüger, J., and Toepel, J., "Influence of femtosecond laser produced nanostructures on biofilm growth on steel," *Applied Surface Science* **418**, 420–424 (2017).

[28] Nastulyavichus, A., Kudryashov, S., Saraeva, I., Smirnov, N., Rudenko, A., Tolordava, E., Zayarny, D., Gonchukov, S., and Ionin, A., "Nanostructured steel for antibacterial applications," *Laser Physics Letters* **17**(1), 016003 (2019).

[29] Guenther, D., Valle, J., Burgui, S., Gil, C., Solano, C., Toledo-Arana, A., Helbig, R., Werner, C., Lasa, I., and Lasagni, A. F., "Direct laser interference patterning for decreased bacterial attachment," in [*Laser-based Micro-and Nanoprocessing X*], **9736**, 216–224, SPIE (2016).